HHS Public Access

Author manuscript

Microvasc Res. Author manuscript; available in PMC 2016 May 01.

Published in final edited form as:

Microvasc Res. 2015 May ; 99: 8–18. doi:10.1016/j.mvr.2015.02.008.

Human brain microvascular endothelial cells resist elongation due to shear stress

Adam Reinitz[1], **Jackson DeStefano**[1], **Mao Ye**, **Andrew D. Wong**, and **Peter C. Searson**[*]

Department of Materials Science and Engineering, Johns Hopkins University, 3400 North Charles Street, Baltimore, MD 21218, USA

Institute for Nanobiotechnology, Johns Hopkins University, 3400 North Charles Street, Baltimore, MD 21218, USA

Abstract

Endothelial cells in straight sections of vessels are known to elongate and align in the direction of flow. This phenotype has been replicated in confluent monolayers of bovine aortic endothelial cells and human umbilical cord endothelial vein cells (HUVECs) in cell culture under physiological shear stress. Here we report on the morphological response of human brain microvascular endothelial cells (HBMECs) in confluent monolayers in response to shear stress. Using a microfluidic platform we image confluent monolayers of HBMECs and HUVECs under shear stresses up to 16 dyne cm^{-2}. From live-cell imaging we quantitatively analyze the cell morphology and cell speed as a function of time. We show that HBMECs do not undergo a classical transition from cobblestone to spindle-like morphology in response to shear stress. We further show that under shear stress, actin fibers are randomly oriented in the cells indicating that there is no cytoskeletal remodeling. These results suggest that HBMECs are programmed to resist elongation and alignment under shear stress, a phenotype that may be associated with the unique properties of the blood–brain barrier.

Keywords

Human brain microvascular endothelial cells; Shear stress; Cell morphology; Elongation; Alignment

Introduction

Blood flow results in a frictional drag, or shear stress, on the endothelial lining of vessel walls parallel to the direction of flow. These stresses play an important role in regulating endothelial cell morphology and function, and in mediating a wide range of signaling and transport processes between the vascular system and surrounding tissue (Aird, 2007a, 2007b; Chien, 2007; Davies, 1995; Johnson et al., 2011).

[*]Corresponding author. searson@jhu.edu (P.C. Searson).

[1]Contributed equally.

Supplementary data to this article can be found online at http://dx.doi.org/10.1016/j.mvr.2015.02.008.

Endothelial cells in straight sections of large resected vessels and away from branch points exhibit an elongated, spindle-like morphology (Davies, 1995; Dolan et al., 2013; Kibria et al., 1980; Levesque et al., 1986; Nerem et al., 1981; Reidy and Langille, 1980; Silkworth and Stehbens, 1975; Zand et al., 1988). When subjected to a physiological shear stress in 2D cell culture, confluent monolayers of bovine aortic endothelial cells (BAEs), human umbilical vein endothelial cells (HUVECs), and primary baboon artery endothelial cells (BAECs) undergo a transition from a cobblestone morphology to an elongated spindle-like morphology and align in the direction of flow (Blackman, 2002; Chien, 2007; Chiu et al., 1998; Davies, 1995; Ensley et al., 2012; Eskin et al., 1984; Levesque and Nerem, 1985, 1989; Malek and Izumo, 1996; Simmers et al., 2007). A similar morphological response has been reported for human abdominal aortic endothelial cells seeded onto the inner surface of a polydimethyl siloxane tube (Farcas et al., 2009; Rouleau et al., 2010). The response of BAEs and HUVECs to shear stress results in a morphology similar to that of endothelial cells in resected vessels, which provides evidence that mechano-transduction modulates cellular function and is important in maintaining vascular homeostasis (Chien, 2007; Johnson et al., 2011).

Morphological parameters associated with endothelial cells in confluent monolayers in response to shear stress and resected vessels are summarized in Table 1. Endothelial cells in straight sections of the aorta across several animal species are characterized by an inverse aspect ratio (IAR, cell width/cell length) of about 0.20, a circularity of about 0.3, and an average orientation angle with respect to the flow direction (θ) of 5–15°. Similar morphological parameters have been reported for 2D confluent monolayers of BAEs and HUVECs in cell culture under shear stress. The somewhat larger variability in morphological parameters seen in cell culture is due in part to the different experimental conditions and the fact that the morphology is often characterized at a single time point.

In previous work we have reported on the influence of curvature on the morphology of endothelial cells. By seeding confluent monolayers of endothelial cells on collagen-coated glass rods of different diameters, we studied the influence of curvature on endothelial cell morphology (Ye et al., 2014). To minimize the effects of curvature, HUVEC cells elongate and align in the axial direction with decreasing diameter. In contrast, human brain microvascular endothelial cells (HBMECs) do not elongate or align in the axial direction but wrap around in the radial direction with little change in morphology as the diameter decreases (Ye et al., 2014). The endothelial cells in the brain microvasculature are highly specialized, with an array of transporters, efflux pumps, and tight junctions that are an important component of the blood–brain barrier, regulating transport into and out of the brain (Wong et al., 2013). These results suggest that HBMECs may also display a unique morphological phenotype.

Elongation and alignment in response to shear stress is thought to be a universal phenotype of endothelial cells. However, our previous work suggests that brain microvascular endothelial cells may be programmed to respond differently to physical stimuli, such as curvature, compared to endothelial cells from larger vessels. Therefore, here we compare the morphological response of HBMECs, representative of brain capillaries, and HUVECs, representative of large vessels, to shear stress. We show that HBMECs do not elongate and

align in response to physiological shear stress. In addition, we show that actin fibers are randomly oriented within HBMECs and do not align with flow. These results suggest that HBMECs are programmed to resist elongation and alignment in response to shear stress. This phenotype may be associated with the unique properties of the blood–brain barrier.

Materials and methods

Microfluidic platform

The microfluidic device (Fig. 1a–b) was fabricated from polydimethylsiloxane (PDMS, Sylgard) using a machined aluminum mold with four rectangular channels connected in series. Each channel was 4 mm wide and 50 mm long, with heights of 390 μm, 450 μm, 550 μm, and 770 μm, respectively. PDMS was poured to fill half of the mold and partially cured at 100°C for 15 min. Nylon spacers (5mm ID, McMaster) forming the bubble traps were placed on top of the PDMS and sealed with a second layer of PDMS cured at 100 °C for 45 min. The PDMS blocking the bubble traps was removed using a 5 mm inner diameter hole punch and the inlets and outlets were made using a 1.50 mm hole punch. The PDMS channels were then plasma bonded to a 50 mm × 75 mm glass microscope slide (Corning). 6.35 mm ID silicon tubing (McMaster) was used to connect the nylon inserts to the caps of the bubble traps, which was a male Luer to hosebarb connector with a female Luer cap (Cole Parmer).

For Poiseuille flow in a rectangular channel, the wall shear stress was given by $\tau = 6Q\mu/h^2w$ where Q was volumetric flow rate, μ was dynamic viscosity, h was channel height, and w was channel width. The channel heights were chosen such that the shear stress in the four channels scales in the ratio 1:2:3:4.

The flow setup was composed of a custom machined Teflon media reservoir connected to 1/8″ ID silicon tubing (McMaster) (Fig. 1a–c). Media from the Teflon reservoir passed through a 1.5 m coil of silicon tubing located in a gas exchange chamber (In Vivo Scientific) of humidified 5% CO_2. The flow was then directed through the microfluidic device and returns to the media reservoir via the programmable peristaltic pump (New Era Pumps, NE-9000). Teflon tubing was used for the return flow from the peristaltic pump to the media reservoir. The peristaltic pump was programmed to gradually increase flow stepwise from 1.25 to 7.5 mL min^{-1} over the first 6 h, increasing by 1.25 mL min^{-1} every hour. After the 6 h ramp up, the flow was maintained at 10 mL min^{-1} which equates to a time average shear stress of 4, 8, 12, and 16 dyne cm^{-2} within four channels respectively. Flow was applied to HBMECs for 36 h and HUVECs for 72 h. Characterization of the flow produced from the peristaltic pump confirms it was pulsatile (see Supplementary Information). The flow rates were verified using a flow meter (Liquid Flowmeter NIST-traceable calibration, Cole Parmer) that measured the output from the microfluidic device to verify the time averaged flow rate. The flow profile was verified by measuring the velocity of fluorescent beads at different heights in the channels (see Supplementary Information for details). For static experiments, cells were seeded into a device and allowed to grow to confluence for 24 h. To avoid depletion of nutrients, the media was briefly circulated approximately every 8 h.

Cell culture

Immortalized human brain microvascular endothelial cells (HBMECs) (Nizet et al., 1997) were cultured in M199 (Sigma-Aldrich) supplemented with 10% fetal bovine serum (FBS) (Invitrogen, Carlsbad, CA) and 1% penicillin streptomycin (Invitrogen). In a comparison of four immortalized human brain microvascular endothelial cell lines, this cell line showed the highest transendothelial electrical resistance values and was determined to be the most suitable for an *in vitro* blood–brain barrier model (Eigenmann et al., 2013). Human umbilical vein endothelial cells (HUVECs) (Promocell, Heidelberg, Germany) were grown in endothelial cell growth medium (EGM-2, Promocell) containing endothelial basal medium (EBM), 2% fetal calf serum (FCS), and 1% penicillin streptomycin, hEGF, hydrocortisone, VEGF, hbFGF, R3 IGF, AA-500, and Heparin. Both cell lines were cultured under physiological conditions on uncoated tissue culture polystyrene flasks (Sarstedt).

Before introducing the cells into the microfluidic device, cells were thoroughly washed twice with PBS without Ca^{2+} or Mg^{2+} (Lonza) and removed from their culture surface using 0.5% EDTA/trypsin (Invitrogen) for 3 min at 37 °C. Prior to seeding cells, the interior walls of the channels were coated with 62.5 μg mL^{-1} fibronectin (BD Biosciences, San Jose, CA) for 1 h at room temperature. HBMECs and HUVECs were introduced at concentrations of 1,500,000 cells mL^{-1} and 2,000,000 cells mL^{-1}, respectively, and grown to confluence in their respective culture media. Each channel was seeded with 100 μL of cell suspension, resulting in 150,000 cells for HBMEC channels and 200,000 cells for HUVEC channels. Prior to applying shear stress, the media was changed to reduced growth factor media composed of EBM supplemented with 2% FCS. The microfluidic device was mounted in a live-cell chamber (In Vivo Scientific) on the microscope, maintained at 37 °C and 5% CO_2. Static experiments were conducted using a similar procedure. Cells were seeded into a device and allowed to grow to confluence for 24 h. At confluence, the flow loop was connected and the media changed to reduced growth factor media. Approximately every 8 h the pump was temporarily activated to slowly circulate nutrients and replace the volume of media within the four channels.

Live-cell and immunofluorescence imaging

Imaging was performed using a Nikon TE-2000U inverted microscope controlled by NIS Elements software (Nikon, Japan). Phase-contrast images were captured every 20 min at three locations in each 50 mm channel: at the center and 10 mm from each end (Fig. 1d). Before each time lapse image the locations were defined using NIS Elements software. The first location is set such that it is 10 mm from the inlet of the channel and directly in the center of the flow, roughly 2 mm from the side walls to avoid edge effects (Fig. 1d). Subsequent locations are spaced 10 mm from each other, resulting in three imaging locations spaced equally over the length of the channel in the laminar flow region. Images were obtained using a 10× Nikon Plan Fluor objective. Each image was 1.5 mm × 1.2 mm and contained 1000–2000 cells. Autofocus adjustment using NIS-Elements is performed before each image capture to account for any z-drift.

Monolayers of endothelial cells within the device were prepared for immunofluorescence staining immediately following the flow experiment by washing with warm PBS with Ca^{2+}

and Mg^{2+} and fixing in 4% formaldehyde (Fisher Scientific) in PBS. Cells were subsequently washed with PBS and permeabilized with 0.1% Triton-X 100 (Sigma Aldrich). Samples were blocked using 10% goat serum in PBS, and incubated with anti-zonula occluden-1 (ZO-1) antibody (rabbit monoclonal 1:200, Invitrogen) for 1 h at room temperature, washed, and incubated with a goat anti-rabbit secondary antibody (1:200, Alexa Fluor 568, Invitrogen). Samples were subsequently stained for F-actin using AlexaFluor 488 phalloidin (Invitrogen) and for nuclei using DAPI (1:2500, Roche Applied Science). Immunofluorescence images were obtained from the same locations as phase contrast images.

Image analysis

Quantitative analysis of cell morphology was performed using ImageJ (NIH, Bethesda, MD). Images of the cell monolayers from the time-lapse movies were imported into ImageJ and the cell borders were obtained automatically using a custom macro (see Supplementary Information for code and user manual). At each time point, images from the three locations were analyzed (Fig. 1d). Each experiment was performed at least three times. Morphological parameters of individual cells were obtained as long as more than 85% of the monolayer could be traced by this method. To validate cell morphology obtained by automated analysis of phase contrast images, the same morphological parameters were obtained by manual analysis of the cell boundaries in immunofluorescence images. Excellent agreement was obtained between the two methods (see Supplementary Information).

Cell motility was evaluated using the MATLAB-based particle image velocimetry application, OpenPIV (Taylor et al., 2010). The software divides each image into a matrix of smaller regions, called interrogation windows, for analysis. Each interrogation window is compared to itself between successive images to analyze the movement of “particles”. In our case, the moving particles are the intracellular features (e.g. vacuoles and organelles) that exhibit contrast in the image and are used to collectively estimate the speed of cells within the endothelial monolayer. The same 1.5 mm × 1.2 mm images obtained at 20 min intervals were used for analysis. The interrogation window was set to 32 pixel × 32 pixel (20.5 μm × 20.5 μm), which was approximately one-fourth the area of a typical endothelial cell. The PIV tool measures velocity from the offset of intracellular features between phase-contrast images at successive time points and assigns each interrogation window a vector to describe the movement of cells within the area. The magnitudes of these vectors, regardless of direction, were averaged to obtain global cell speed within the monolayer. While PIV is not a direct measurement of cell speed, the results were compared to the speed determined by manually tracking individual cells within the endothelial monolayer. The PIV speed exhibits similar magnitude and captures the same trends as manually tracked cells (see Supplementary Information).The influence of image analysis parameters (image size, interrogation window size, sampling time, and the space between analyzed points) on PIV magnitude was summarized in Supplementary Information.

The distribution of actin stress fibers was quantified using Fourier transform analysis (Lee and Chen, 2002; Ye et al., 2014). Cell monolayers were fixed and stained as described previously (Ye et al., 2014) and the actin (green) channel of immunofluorescence images

was converted to grayscale. The images were cropped to be 884 μm × 884 μm and FFTs were performed using the FFT2 routine in MATLAB. For directional textures the Fourier spectrum of the image will concentrate in certain directions, as opposed to random orientation with non-directional textures. Two eigenvalues are calculated from the Fourier spectrum and based on the ratio of these eigenvalues the directionality can be determined. For directional textures the larger eigenvalue will be much greater than the smaller eigenvalue, thus the ratio will be large (van der Meer et al., 2010). The resulting intensity distributions in the frequency domain were converted to radial intensity distributions from 0 to 180° at 10° increments (see Supplementary Information). We defined the intensity in the range 0 ± 10° as the fraction of fibers parallel to the flow direction, and the intensity in the range 90 ± 10° as the fraction of fibers perpendicular to the flow direction.

Western blot

Lysates of HBMECs and HUVECs cultured in the microfluidic device were isolated by removing the PDMS directly above each channel. The exposed channels were rinsed 3 times with ice-cold PBS (Corning) and lysed with radioimmunoprecipitation assay (RIPA, 150 mM NaCl, 1.0% IGEPAL® CA-630, 0.5% sodium deoxycholate, 0.1% SDS, and 50 mM Tris, pH 8.0) buffer supplemented with a protease inhibitor cocktail (Sigma Aldrich) containing 2 mM 4-(2-aminoethyl)benzenesulfonyl fluoride (AEBSF), 0.3 μM aprotinin, 130 μM bestatin, 1 mM ethylenediaminetetraacetic acid (EDTA), 14 μM E-64, and 1 μM leupeptin. Lysed cells were scraped from the surface of the channel and centrifuged at 25,000 rpm for 25 min at 4 °C. A solution containing 40 μL of cell lysate, 8 μL NuPage (LifeTech) 10× sample reducing buffer, and 16 μL NuPage (Life Technologies, Frederick, MD) 4× LDS sample buffer was incubated for 15 min in a 90 °C water bath. Protein samples were separated on a 4–15% Bio-Rad Mini-Protean TGX gel in a Bio-Rad Mini-Protean Tetra System gel electrophoresis chamber and transferred to a nitrocellulose membrane using the Bio-Rad Transblot Turbo system. The membranes were blocked at room temperature for 1 h in tris-buffered saline containing 0.5% Tween 20 (TBST) and 5% non-fat dry milk. The membranes were then incubated in the blocking solution with primary antibodies overnight at 4 °C. Immunoblotting was performed using 1:500 polyclonal rabbit anti-ZO-1 (Invitrogen), 1:1000 monoclonal mouse anti-beta-catenin (BD Biosciences), and 1:1000 polyclonal rabbit anti-beta-actin (Cell Signaling Technology) as a loading control. The membranes were washed three times with TBST and incubated with 1:3000 anti-mouse and anti-rabbit horseradish peroxidase secondary antibody for 1 h at room temperature. The membranes were washed three times with TBST and incubated for 3 min in SuperSignal West Pico Chemiluminescent Substrate. The membranes were then imaged using the Bio-Rad Chemidoc molecular imaging station.

Results and discussion

The brain microvascular endothelial cells that form the lumen of brain capillaries are an important component of the blood–brain barrier that regulates homeostasis in the brain. The flow rate in brain capillaries is typically 6–12 nL min^{-1}, corresponding to shear stresses of 10–20 dyne cm^{-2} (Davies, 1995; Kamiya et al., 1984). These stresses are also thought to

play an important role in regulation of the blood–brain barrier (Cucullo et al., 2011; Krizanac-Bengez et al., 2004; Neuwelt et al., 2008; Tarbell, 2010).

HBMECs and HUVECs were seeded in our microfluidic platform until reaching confluence, typically 24 h for both HBMECs and HUVECs. After reaching confluence, the media was changed to endothelial basal media supplemented with 2% FCS, and the flow rate was monotonically increased over 6 h resulting in a final respective shear stress of 4, 8, 12, and 16 dyne cm^{-2} within each channel of differing height. When kept under physiological conditions, the microfluidic platform could maintain confluent monolayers under these shear stresses for longer than 4 days.

HBMECs in confluent monolayers exhibit a cobblestone morphology with no evidence of elongation or alignment after 36 h exposure to physiological shear stress (Fig. 2). At low shear stress, the cell monolayers become very compact and exhibit overgrowth, whereas at the higher shear stress, the monolayers are noticeably less dense and exhibit much less overgrowth (Supplementary Video 1).

In contrast, HUVEC monolayers develop a cobblestone morphology 7–17 h after applying shear stress, and subsequently show a transition to a spindle-like morphology after 24 h (Supplementary Video 2). The degree of orientation and alignment of the spindle-like morphology increases with increasing shear stress (Fig. 2). These results are similar to previous studies of HUVECs (Blackman, 2002; Simmers et al., 2007) and bovine aortic endothelial cells (BAEs) (Dewey et al., 1981; Levesque and Nerem, 1985) under physiological shear stress.

Quantitative analysis of cell morphology

The observed morphological changes were quantitatively analyzed in terms of the inverse aspect ratio (IAR), the orientation angle (θ), and the average projected cell area (A). The IAR is obtained from the length of the short axis divided by length of long axis (Fig. 1f), and is a measure of cell elongation. IAR was preferred over circularity since the cell–cell boundaries are not well defined in the phase contrast images. The orientation angle is the measured angle between the long axis of a cell and the flow direction. The cell area is the 2D projected area covered by the automatically traced cell. The time dependence of these morphological parameters was determined from time-lapse videos and verified from analysis of immunofluorescence images (see Supplementary Information). In this section we summarize the steady state morphological response of the monolayers after 36 and 72 h; in the next section, we describe their transient responses.

For HBMECs the IAR is about 0.64, independent of exposure time and shear stress (Fig. 3a), showing that the cells do not elongate after 36 h at physiological shear stress. The average orientation angle after 36 h is about 45°, characteristic of a random distribution of orientation angles, and is also independent of shear stress (Fig. 3b). These results support the consistent observations from the phase contrast images (Fig. 2) that HBMEC cells do not elongate or align under shear stress. In contrast, the cell area is dependent on shear stress, increasing from less than 1000 μm^2 at 4 dyne cm^{-2} to 1490 μm^2 at 16 dyne cm^{-2} at −6 h. Increasing shear stress may improve contact inhibition between endothelial cells while

physically removing overgrown cells with poor adhesion to the glass surface; this is discussed further below. The resistance of the HBMECs to morphological change due to shear stress is surprising since elongation and alignment is a hallmark of endothelial cells, especially those derived from large vessels. However, other cell types, such as smooth muscle cells do not exhibit morphological changes in response to shear stress (Malek et al., 1994).

HUVECs show a noticeable decrease in IAR and orientation angle with increasing shear stress after 36 h. The average IAR decreases from 0.60 under static conditions to 0.49 under 16 dyne cm^{-2} shear stress (Fig. 3a). The average orientation angle decreases from 43° under static conditions to 23° under 16 dyne cm^{-2} shear stress (Fig. 3b). After 72 h of flow, the HUVECs show a further decrease in IAR from 0.61 under static conditions to 0.41 under 16 dyne cm^{-2} shear stress (Fig. 3a). Reported values of IAR *in vivo* range from 0.14 to 0.2 while *in vitro* measurements range from 0.24 to 0.72 (Table 1). The HUVEC steady state IAR of 0.41 is consistent with these observations. Similarly, the average orientation angle decreases from 44° under static conditions to 17° under 16 dyne cm^{-2} shear stress (Fig. 3b). Reported values of *in vivo* orientation angle range from 4.5 to 15° while *in vitro* measurements range from 14 to 55° (Table 1). The HUVEC steady state value of 17° is within this range. The average area for HUVECs was about 1500 μm^2 under shear stress (Fig. 3c), somewhat smaller than the average area under static conditions.

Our HUVEC *in vitro* results agree with reported *in vivo* and *in vitro* morphological parameters. HUVECs had a steady state IAR of 0.41 which is in agreement with IAR of endothelial cells in the pulmonary vein *in vivo*.[10] Along with elongation, HUVECs also increased their alignment under applied shear stress. HUVECs at steady state had an orientation angle of 17° which is only slightly larger than the reported *in vivo* values. In contrast HBMECs showed no elongation or orientation with flow. With a steady state IAR of 0.65, HBMECs are more circular than those reported *in vivo*, and have similar IAR to *in vitro* cells under static conditions. There is also no change in the orientation of these cells. At steady state HBMECs have an orientation of 45°, which represents collectively random alignment. This is in contrast to large vessel *in vivo* reports[7,9,10] and agrees with values reported for HBMECs *in vitro* under static conditions.

Transient response

The inverse aspect ratio of HBMECs in confluent monolayers remains about 0.65 after 36 h under both static conditions and for shear stresses of 4, 8, 12, and 16 dyne cm^{-2} (Fig. 4a). Similarly, the average orientation angle was about 45°, independent of time and shear stress (Fig. 4b).

The average area for HBMECs is dependent on shear stress (Fig. 4c). The cell area after 6 h pre-conditioning (from −6 to 0h), increases from about 1000 μm^2 under 4 dyne cm^{-2} up to about 1490 μm^2 under 16 dyne cm^{-2} shear stress. Under 4, 8, and 12 dyne cm^{-2}, the cell area decreases monotonically with time highlighting the fact that proliferation is not completely inhibited upon reaching confluence. In contrast, under 16 dyne cm^{-2} shear stress, the cell area remains approximately constant with time; this may be due to improved contact inhibition regulated by the higher shear stress or the physical removal of overgrown

cells from the monolayer. Removal of cells, as well as flattening and spreading, would result in an increase in average cell area. For HBMECs, we observe relatively no change or a slight decrease in average cell area under all shear stress conditions which is consistent with no change or a slight increase in the number of adherent cells. Phase contrast movies show that shear stress removes overgrown cells and to a larger degree under 16 dyne cm^{-2} (Supplementary Video 1).

HUVEC cells in confluent monolayers exhibit a pronounced transient response to an applied shear stress (Fig. 4d–f). After pre-conditioning, the HUVECs are slightly elongated with an IAR of 0.55 (Fig. 4d), and close to randomly oriented with an average orientation angle of about 41° (Fig. 4e). During the first few hours under sustained shear stress, the HUVECs develop a distinct cobblestone morphology that is accompanied by a small increase in IAR as the cells become more rounded. The IAR reaches a maximum after 15–20h depending on the magnitude of the shear stress. At longer times, there is a transition from the cobblestone morphology to an elongated spindle-like morphology and alignment in the direction of flow, characterized by an IAR of about 0.40 after 72 h. The time dependence of the average orientation angle is similar, with an initial increase followed by a decrease to values of 15–20° after 72 h. An IAR of 0.4 corresponds to an elongation of 250%, and orientation angles of 15–20° indicate that cells are strongly aligned in the direction of flow.

The average area of HUVEC cells decreases slightly with time from about 1900 μm^2 to about 1500 μm^2 within the first 12 h and then remains constant independent of shear stress (Fig. 4f). This decrease in cell area is associated with the development of a cobblestone morphology and implies a 25% increase in the number of cells. Once the cobblestone morphology is established, contact inhibition results in a constant cell area during the transition to an elongated spindle-like morphology.

The morphological data for HUVECs reported here are similar to previous reports for BAEs and HUVECs (Table 1) (Blackman, 2002; Levesque and Nerem, 1985; Simmers et al., 2007). Detailed comparison of the dynamic response is difficult since most shear stress experiments on confluent monolayers are performed at two time points; typically 0 and 24 h after exposure to shear flow. The time dependence of the morphology of HUVECs in response to 7.5 dyne cm^{-2} recorded up to 96 h (Simmers et al., 2007) suggests that a steady state morphology is not reached even after 4 days. Similarly, the circularity of BAEs does not reach a steady state after 48 h exposure to a shear stress of 60 dyne cm^{-2} (Levesque and Nerem, 1989). We observe a transition from cobblestone to spindle-like morphology, with the cobblestone morphology observed 7–17 h after the onset of the shear stress, and the spindle-like morphology established after 24 h. Previous reports show that the transition between cobblestone and spindle-like morphology occurs after 12–24 h (Blackman, 2002; Dewey et al., 1981; Levesque and Nerem, 1985, 1989; Simmers et al., 2007).

Cell speed

To quantify the activity of HBMEC and HUVEC monolayers under shear stress, we used particle imaging velocimetry (PIV). The HBMECs exhibit an initial increase in speed during pre-conditioning which continues until about 5 h after exposure to maximum shear stress (Fig. 5a). The PIV speed peaks at 0.3 $\mu m\ min^{-1}$ and subsequently decreases to about 0.2 μm

min^{-1} after about 36 h. The time dependence of the cell speed in HBMEC monolayers is independent of shear stress and is not correlated with morphological changes (Fig. 4a–c). Despite the lack of morphological changes observed for the HBMECs, PIV speeds indicate that mechanical forces applied through shear stress result in transient changes in cell speed. These measurements were validated by manually tracking individual cells (see Supplementary Information).

The PIV speed of HUVECs also exhibits an initial increasing to a maximum after about 5 h under shear stress and then decreases to a steady state value of about 0.1 μm min^{-1} after 24 h (Fig. 5b). As for the HBMEC monolayers, there is no clear dependence of speed on shear stress. The steady state magnitude of the HBMEC monolayers is about double that of the HUVEC monolayers, suggesting that they are considerably more active.

The PIV measurements show that shear stress results in a transient increase in monolayer activity followed by a relaxation to a steady state value after about 24 h. HBMECs retain a cobblestone morphology (Fig. 2a–f) and do not exhibit elongation and alignment (Figs. 3a–c and 4a–c); this is reflected by their PIV speeds that show a modest decrease in magnitude. In contrast, HUVEC monolayers exhibit a transition from a cobblestone to spindle-like morphology (Fig. 2g–l) while elongating and orienting in the direction of flow (Figs. 3a–c and 4d–f); their development of a spindle-like morphology appears correlated with a decrease in monolayer activity (Fig. 5b).

Cytoskeletal reorganization

To further investigate the differences in morphology and monolayer activity, we examined the organization of the actin cytoskeleton. Actin filaments in HBMECs and HUVECs are prominent and distinct (Fig. 6), typical of cells on rigid substrates (Tojkander et al., 2012). The actin filaments in HBMECs after 36 h under shear stress show a dense actin network within the cell body but no obvious preferential alignment with the direction of flow (Fig. 6a–c). At the lowest shear stress the actin filaments are somewhat indistinct, however, at higher shear stresses the actin filaments become well defined bundles of fibers. At these higher shear stresses, the actin filaments within each cell are often aligned, although the alignment is not biased in the direction of flow.

The actin filaments in HUVECs are located both in the cell and concentrated at the cell–cell boundaries (Fig. 6d–f). With increasing shear stress, the filaments become more distinct with noticeable localization at the cell–cell boundaries. These observations are consistent with our current understanding of endothelial cytoskeletal reorganization in response to shear stress. BAEs exposed to shear stress have been shown to increase the localization of microfilaments and intermediate filaments along their peripheries (Galbraith and Sheetz, 1998). Under steady laminar flow, HUVECs also form thick actin bundles that span the cell body and are aligned in the direction of flow (Blackman, 2002; Galbraith and Sheetz, 1998; Girard and Nerem, 1995). However, under pulsatile flow, HUVEC monolayers reduce the presence of centrally oriented stress fibers, and retain a thin cortical fiber structure (Blackman, 2002). Since the flow rate within our device is pulsatile, fluctuating between approximately 0–14 mL min^{-1} (Supplementary Fig. S2), with increasing shear stress we also see retention of peripherally located actin filaments within HUVEC monolayers with fewer

stress fibers traversing the length of the cell. In contrast, HBMECs form thicker actin bundles across the cell body that are not aligned with the direction of flow; this is consistent with their resistance to shear-induced changes to IAR and cell orientation (Fig. 4a–b).

To quantitatively characterize the orientation and alignment of actin fibers,weuse a Fourier transform method (Lee and Chen, 2002) that has been adapted to characterize the orientation and alignment of collagen fibers (Chaudhuri et al., 1987; Ng et al., 2005; van Zuijlen et al., 2002) and actin filaments (van der Meer et al., 2010; Ye et al., 2014) in individual cells. Grayscale immunofluorescence images are Fourier transformed to obtain a radial intensity distribution (see Supplementary Information) (Ng et al., 2005; van Zuijlen et al., 2002); we determine the fraction of radial intensities in the range 0 ± 10° and 90 ± 10°, corresponding to the fraction of filaments aligned parallel and perpendicular to the flow direction respectively. Using these ±10° bins, the intensity for a random orientation of filaments is 11.1% (100%/9 bins).

The intensity of actin filaments in HBMECs is about 11% in both the parallel and perpendicular directions at all shear stresses, confirming a random distribution of filaments (Fig. 6g). For HUVECs, the intensity distributions under 8 and 12 dyne cm^{-2} are 12.8% and 12.4%, respectively, indicating some preferential alignment in the direction of flow. Under 16 dyne cm^{-2}, the parallel intensity distribution increases to 15.1%, indicating strong alignment in the flow direction. The corresponding perpendicular intensity distributions for HUVECs are lower than that of a random distribution of filaments with values of 9.1%, 9.7%, and 8.2% at 8, 12, and 16 dyne cm^{-2}, respectively (Fig. 6h).

Protein expression

To provide an independent measurement of cell morphology, HBMEC and HUVEC monolayers were stained for zona occludin-1 (ZO-1), a tight junction protein expressed in both cell lines and localized to the cell–cell junctions (Beese et al., 2010; Bhattacharya et al., 2008; Lee et al., 2006; Man et al., 2008; Ye et al., 2014). On forming a confluent monolayer of HBMECs and prior to applying a shear stress, ZO-1 expression at the cell–cell junctions is clearly delineated in addition to being expressed in the nucleus (Fig. 7a), consistent with previous reports (Man et al., 2008; Ye et al., 2014). After 36 h, under static conditions or under flow, ZO-1 expression at the cell–cell junctions becomes punctate and expression in the nucleus becomes less pronounced, independent of shear stress (Fig. 7b–f).

In contrast, HUVEC monolayers show ZO-1 expression at the cell–cell junctions, the nucleus, and to a lesser extent throughout the cell body. The cell–cell junctions are sharp, relatively straight, and independent of shear stress or time (Fig. 7g–n). Quantitative analysis of the immunofluorescence intensity within the cell body and in the vicinity of the cell–cell junctions (data not shown) revealed no significant differences in ZO-1 localization, independent of the magnitude of the shear stress or time.

For the HBMEC monolayers there is no change in cell morphology with shear stress or time (Figs. 3 and 4), and yet expression of the tight junction protein ZO-1 decreases noticeably at the cell–cell junctions (Fig. 7b–f). In contrast, ZO-1 expression at the cell–cell junctions is well defined in the HUVECs which show both shear stress and time-dependent morphology.

To characterize the expression of junctional proteins ZO-1 and beta-catenin in HBMEC and HUVEC monolayers, we ran western blots after 36 h under flow or no flow conditions (Fig. 8). For HBMEC monolayers, the expression of ZO-1 and beta-catenin increased under flow compared to static conditions, however, there was no clear correlation with immunofluorescence images (Fig. 7). While the relative intensity of ZO-1 and beta-catenin decreased with increasing shear stress (Fig. 8e), there was no statistical significance between measurements. For HUVEC mono-layers, there was no significant change in expression of beta-catenin under flow (Fig. 8f). Although the relative intensity of ZO-1 expression increased with increasing shear stress, there was no statistical significance between measurements.

Conclusions

HBMECs in confluent monolayers do not show the classical transition from cobblestone to spindle-like morphology in response to shear stress. Morphological parameters, specifically inverse aspect ratio and orientation angle, do not change over 36 h when HBMECs are subjected to shear stresses up to 16 dyne cm^{-2}. While there is no change in cell morphology, the cell area decreases slightly with time, indicating net proliferation in the monolayer. This net proliferation suggests that the HBMECs are activated, which is consistent with their cell speed that reaches a maximum at about 5 h, similar to HUVECs, but maintains a higher baseline magnitude. Analysis of the actin cytoskeleton reveals that actin fibers in HBMECs are randomly oriented indicating that there is no cytoskeletal remodeling in response to shear stress. These characteristics are in contrast to HUVECs which show pronounced cell orientation and alignment in the direction of flow, and cytoskeletal remodeling with actin filaments strongly aligned in the direction of flow. These results suggest that HBMECs are programmed to resist elongation and alignment under shear stress.

Supplementary Material

Refer to Web version on PubMed Central for supplementary material.

Acknowledgments

The authors gratefully acknowledge support from NIH (R01CA170629).

References

Aird WC. Phenotypic heterogeneity of the endothelium: I. Structure, function, and mechanisms. Circ Res. 2007a; 100:158–173. [PubMed: 17272818]

Aird WC. Phenotypic heterogeneity of the endothelium: II Representative vascular beds. Circ Res. 2007b; 100:174–190. [PubMed: 17272819]

Beese M, et al. Effect of cAMP derivates on assembly and maintenance of tight junctions in human umbilical vein endothelial cells. BMC Cell Biol. 2010; 11:68. [PubMed: 20822540]

Bhattacharya R, et al. The neurotransmitter dopamine modulates vascular permeability in the endothelium. J Mol Signal. 2008; 3:14. [PubMed: 18662404]

Blackman BR. A new *in vitro* model to evaluate differential responses of endothelial cells to simulated arterial shear stress waveforms. J Biomech Eng. 2002; 124:397. [PubMed: 12188206]

Chaudhuri S, et al. A Fourier domain directional filtering method for analysis of collagen alignment in ligaments. IEEE Trans Biomed Eng. 1987; 34:509–518. [PubMed: 3610201]

Chien S. Mechanotransduction and endothelial cell homeostasis: the wisdom of the cell. Am J Physiol Heart Circ Physiol. 2007; 292:H1209–H1224. [PubMed: 17098825]

Chiu JJ, et al. Effects of disturbed flow on endothelial cells. J Biomech Eng. 1998; 120:2–8. [PubMed: 9675673]

Cucullo L, et al. The role of shear stress in blood–brain barrier endothelial physiology. BMC Neurosci. 2011; 12:15. [PubMed: 21269499]

Davies PF. Flow-mediated endothelial mechanotransduction. Phys Rev. 1995; 75:519–560.

Dewey CF, et al. The dynamic response of vascular endothelial cells to fluid shear stress. J Biomech Eng. 1981; 103:177–185. [PubMed: 7278196]

Dolan JM, et al. High wall shear stress and spatial gradients in vascular pathology: a review. Ann Biomed Eng. 2013; 41:1411–1427. [PubMed: 23229281]

Eigenmann DE, et al. Comparative study of four immortalized human brain capillary endothelial cell lines, hCMEC/D3, hBMEC, TY10, and BB19, and optimization of culture conditions, for an *in vitro* blood–brain barrier model for drug permeability studies. Fluids Barriers CNS. 2013; 10:33. [PubMed: 24262108]

Ensley AE, et al. Fluid shear stress alters the hemostatic properties of endothelial outgrowth cells. Tissue Eng Part A. 2012; 18:127–136. [PubMed: 21787250]

Eskin SG, et al. Response of cultured endothelial-cells to steady flow. Microvasc Res. 1984; 28:87–94. [PubMed: 6748961]

Farcas MA, et al. The development of 3-D, *in vitro*, endothelial culture models for the study of coronary artery disease. Biomed Eng Online. 2009; 8

Galbraith CG, Sheetz MP. Forces on adhesive contacts affect cell function. Curr Opin Cell Biol. 1998; 10:566–571. [PubMed: 9818165]

Girard PR, Nerem RM. Shear stress modulates endothelial cell morphology and F-actin organization through the regulation of focal adhesion-associated proteins. J Cell Physiol. 1995; 163:179–193. [PubMed: 7534769]

Johnson BD, et al. Mechanotransduction of shear in the endothelium: basic studies and clinical implications. Vasc Med. 2011; 16:365–377. [PubMed: 22003002]

Kamiya A, et al. Adaptive regulation of wall shear stress optimizing vascular tree function. Bull Math Biol. 1984; 46:127–137. [PubMed: 6713148]

Kibria G, et al. Pulmonary endothelial pavement patterns. Thorax. 1980; 35:186–191. [PubMed: 7385090]

Krizanac-Bengez L, et al. The cerebral vasculature as a therapeutic target for neurological disorders and the role of shear stress in vascular homeostatis and pathophysiology. Neurol Res. 2004; 26:846–853. [PubMed: 15727268]

Lee KL, Chen LH. A new method for coarse classification of textures and class weight estimation for texture retrieval 1. Pattern Recognit Image Anal. 2002; 12:400–410.

Lee YR, et al. MCP-1, a highly expressed chemokine in dengue haemorrhagic fever/dengue shock syndrome patients, may cause permeability change, possibly through reduced tight junctions of vascular endothelium cells. J Gen Virol. 2006; 87:3623–3630. [PubMed: 17098977]

Levesque MJ, Nerem RM. The elongation and orientation of cultured endothelial-cells in response to shear-stress. J Biomech Eng, Transac ASME. 1985; 107:341–347.

Levesque MJ, Nerem RM. The study of rheological effects on vascular endothelial cells in culture. Biorheology. 1989; 26:345–357. [PubMed: 2605338]

Levesque MJ, et al. Correlation of endothelial-cell shape and wall shear-stress in a stenosed dog aorta. Arteriosclerosis. 1986; 6:220–229. [PubMed: 3954676]

Malek AM, Izumo S. Mechanism of endothelial cell shape change and cytoskeletal remodeling in response to fluid shear stress. J Cell Sci. 1996; 109:713–726. [PubMed: 8718663]

Malek AM, et al. Endothelial expression of thrombomodulin is reversibly regulated by fluid shear-stress. Circ Res. 1994; 74:852–860. [PubMed: 8156632]

Man S, et al. Human brain microvascular endothelial cells and umbilical vein endothelial cells differentially facilitate leukocyte recruitment and utilize chemokines for T cell migration. Clin Dev Immunol. 2008; 2008:384982. [PubMed: 18320011]

Nerem RM, et al. Vascular endothelial morphology as an indicator of the pattern of blood-flow. J Biomech Eng, Transac ASME. 1981; 103:172–176.

Neuwelt E, et al. Strategies to advance translational research into brain barriers. Lancet Neurol. 2008; 7:84–96. [PubMed: 18093565]

Ng CP, et al. Interstitial fluid flow induces myofibroblast differentiation and collagen alignment *in vitro*. J Cell Sci. 2005; 118:4731–4739. [PubMed: 16188933]

Nizet V, et al. Invasion of brain microvascular endothelial cells by group B streptococci. Infect Immun. 1997; 65:5074–5081. [PubMed: 9393798]

Reidy MA, Langille BL. The effect of local blood flow patterns on endothelial cell morphology. Exp Mol Pathol. 1980; 32:276–289. [PubMed: 7379981]

Rouleau L, et al. Endothelial cell morphologic response to asymmetric stenosis hemodynamics: effects of spatial wall shear stress gradients. J Biomec Eng-Transac Asme. 2010; 132

Silkworth JB, Stehbens WE. Shape of endothelial cells in en-face preparations of rabbit blood-vessels. Angiology. 1975; 26:474–487.

Simmers MB, et al. Arterial shear stress regulates endothelial cell-directed migration, polarity, and morphology in confluent monolayers. Am J Physiol Heart Circ Physiol. 2007; 293:H1937–H1946. [PubMed: 17586613]

Tarbell JM. Shear stress and the endothelial transport barrier. Cardiovasc Res. 2010; 87:320–330. [PubMed: 20543206]

Taylor ZJ, et al. Long-duration time-resolved PIV to study unsteady aerodynamics. IEEE Trans Instrum Meas. 2010; 59:3262–3269.

Tojkander S, et al. Actin stress fibers—assembly, dynamics and biological roles. J Cell Sci. 2012; 125:1855–1864. [PubMed: 22544950]

van der Meer AD, et al. Analyzing shear stress-induced alignment of actin filaments in endothelial cells with a microfluidic assay. Biomicrofluidics. 2010; 4:011103.

van Zuijlen PPM, et al. Morphometry of dermal collagen orientation by Fourier analysis is superior to multi-observer assessment. J Pathol. 2002; 198:284–291. [PubMed: 12375260]

Wong AD, et al. The blood–brain barrier: an engineering perspective. Front Neuroeng. 2013; 6:7. [PubMed: 24009582]

Ye M, et al. Brain microvascular endothelial cells resist elongation due to curvature and shear stress. Sci Reports. 2014; 4:4681.

Zand T, et al. Endothelial adaptations in aortic-stenosis–correlation with flow parameters. Am J Pathol. 1988; 133:407–418. [PubMed: 3189514]

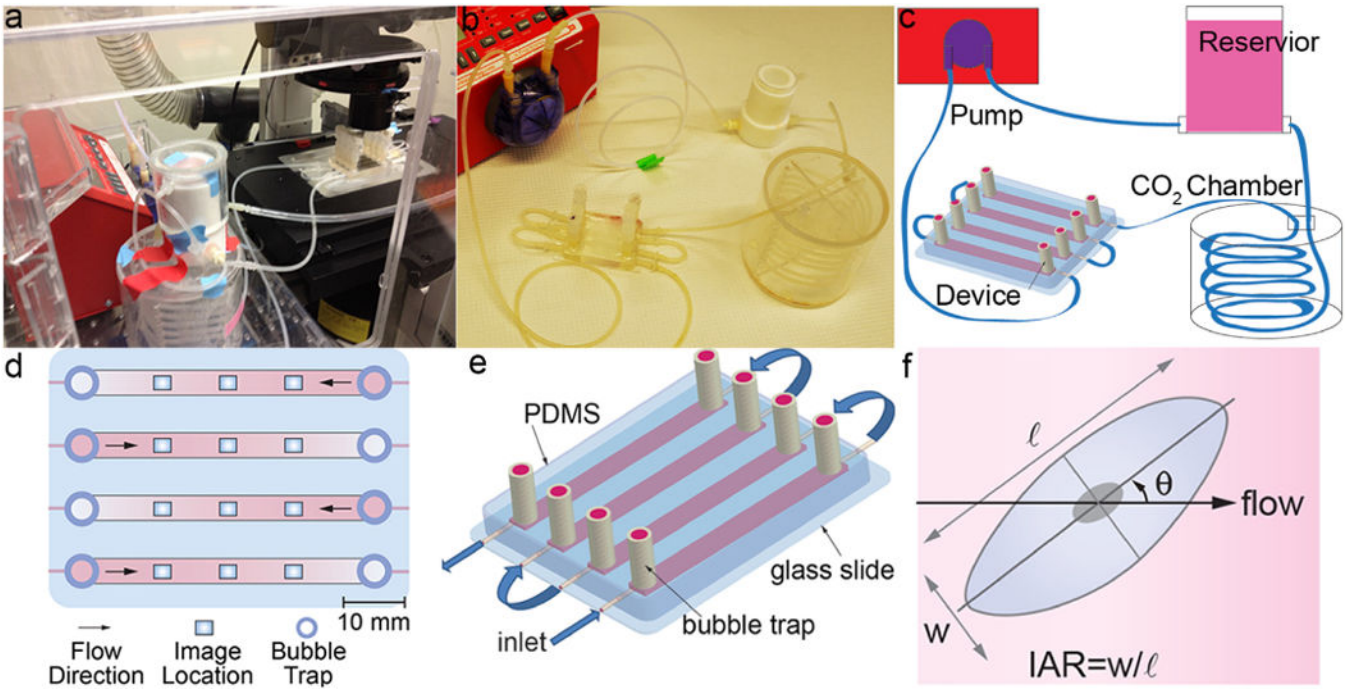

Fig. 1.

(a) Flow system assembled on the microscope stage in the live cell chamber. (b) Flow system assembled on a lab bench. (c) Schematic illustration of the flow system. (d) Schematic illustration of the device showing imaging locations. (e) Schematic illustration of the microfluidic flow device. (f) Morphological parameters include: orientation angle with respect to the flow direction (θ), inverse aspect ratio (IAR) defined as the length of the short axis (w) divided by the length of the long axis (ℓ).

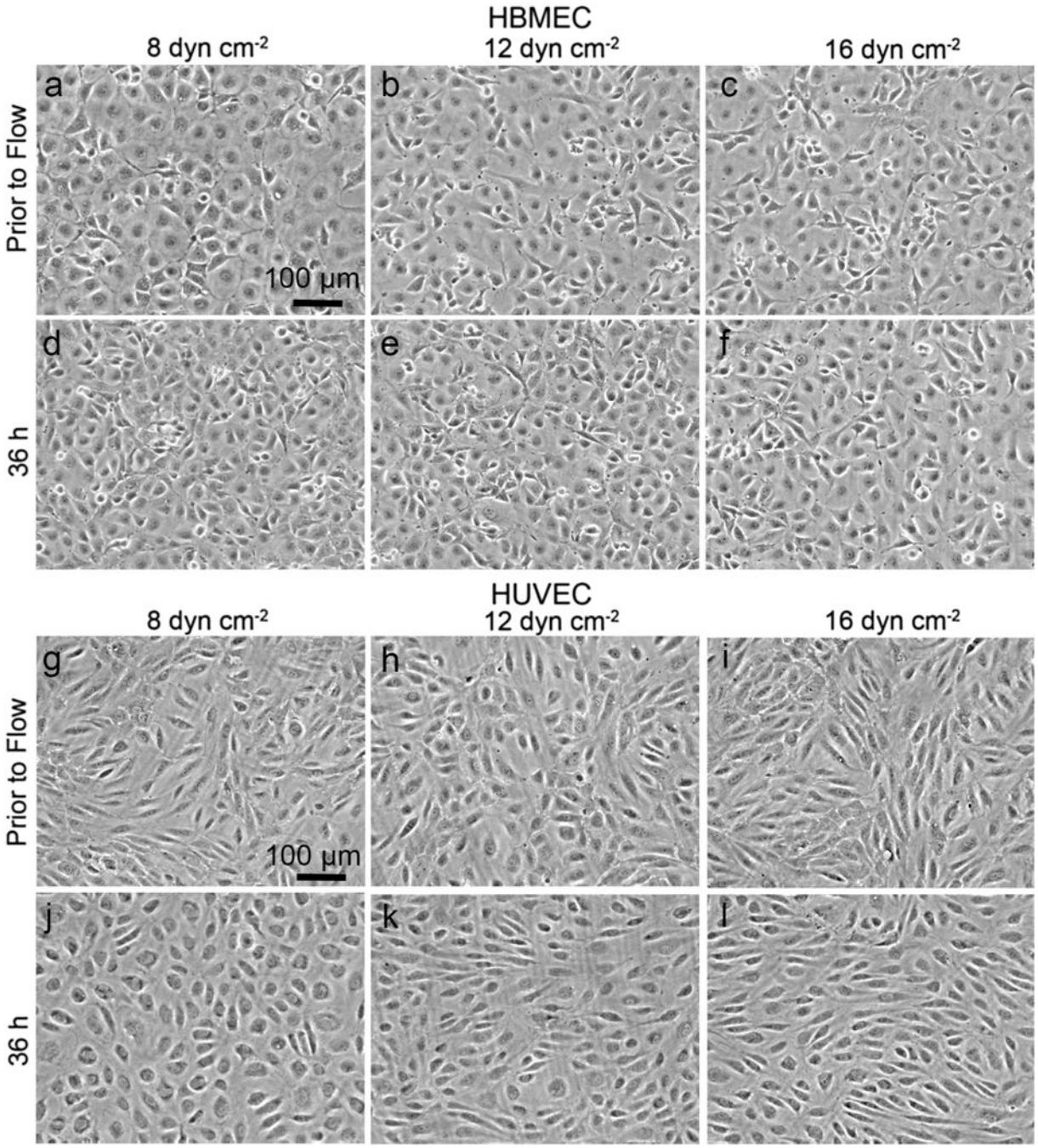

Fig. 2.

Influence of shear stress on confluent monolayers of HBMECs and HUVECs. Phase contrast images of HBMECs and HUVECs: (a–f) HBMECs before and after 36 h of flow at 8, 12, and 16 dyne cm^{-2}, and (g–l) HUVECs before and after 36 h of flow at 8, 12, and 16 dyne cm^{-2}. The direction of flow was horizontal from left to right.

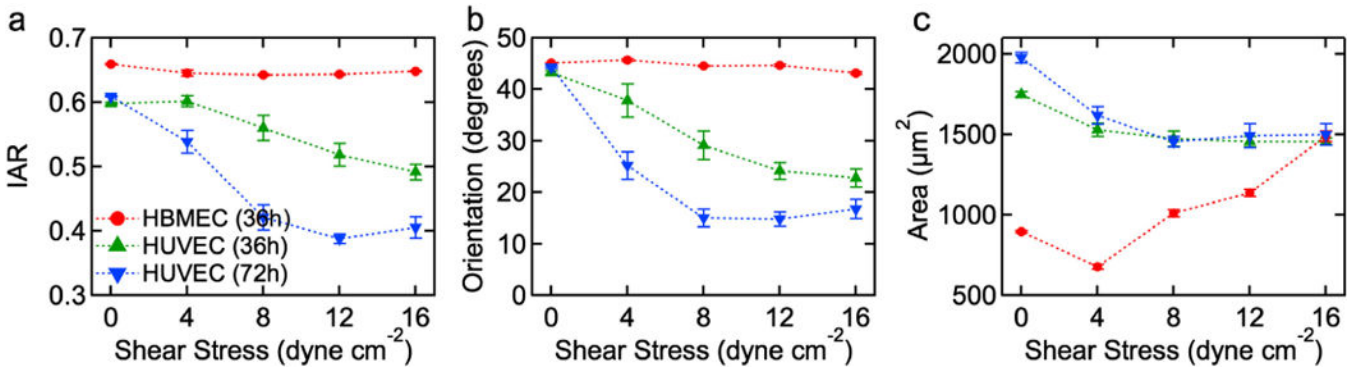

Fig. 3.

HBMECs do not show the characteristic elongation and alignment in response to shear stress. Summary of the morphology of HBMECs and HUVECs in confluent monolayers after exposure to a sustained shear stress of 0, 4, 8, 12, and16 dyne cm^{-2}. (a) Average inverse aspect ratio (IAR), (b) average orientation angle (θ), and (c) average cell area. In each experiment, data were obtained from analysis of three 1.5 mm × 1.2 mm images, corresponding to 1000–2000 cells. All experiments were performed in triplicate. Error bars represent SE.

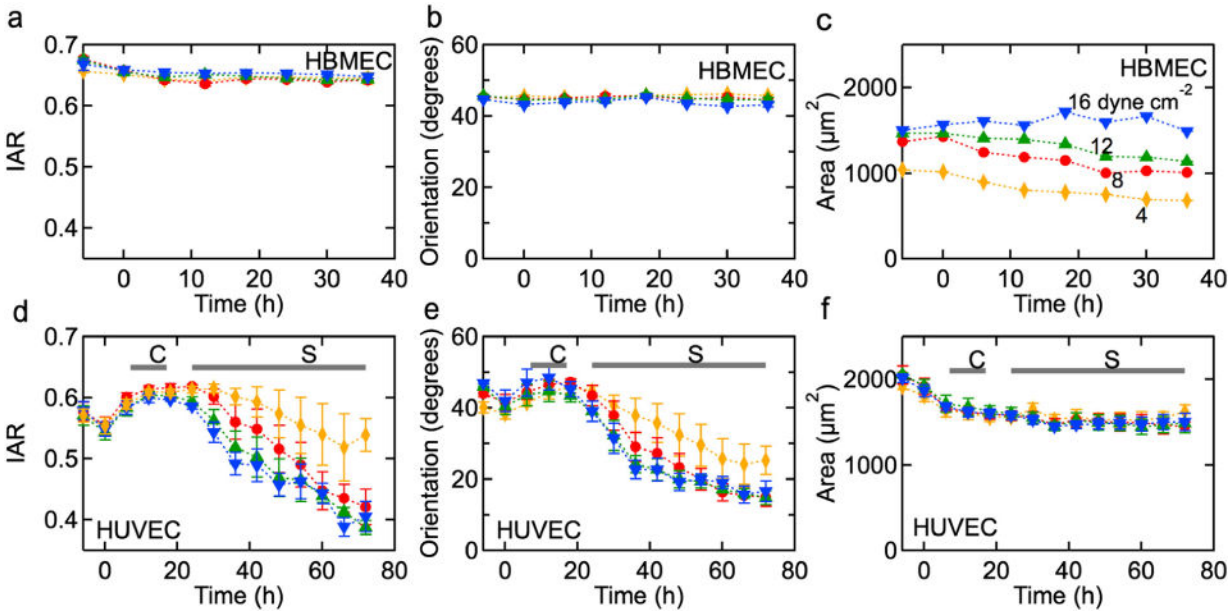

Fig. 4.

Representative time dependence of morphology parameters under 4, 8, 12, and 16 dyne cm^{-2} shear stress. HBMECs: (a) inverse aspect ratio (IAR), (b) average angular orientation (θ), and (c) average cell area (A). HUVEC: (d) IAR, (e) average angular orientation, and (f) area. The horizontal bars indicate when a well defined cobblestone (C) or spindle-like (S) morphology is observed.

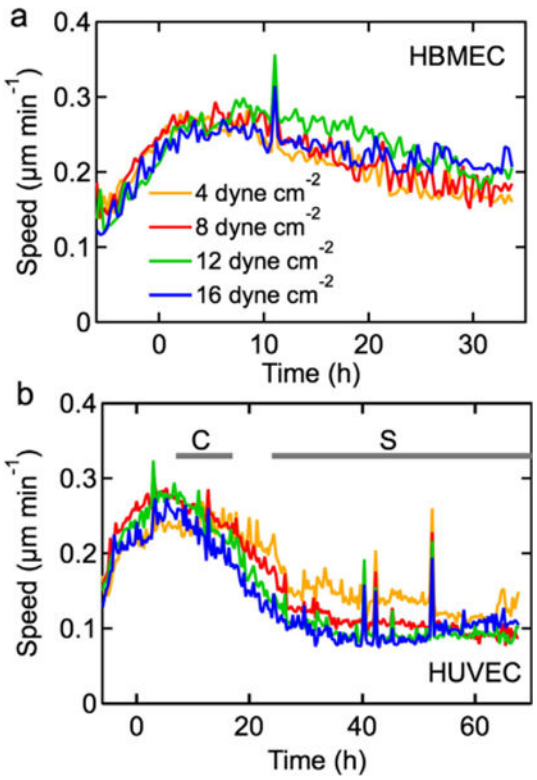

Fig. 5.

Average speed in confluent monolayers exposed to a shear stress of 4, 8, 12, and 16 dyne cm^{-2}. (a) HBMECs, and (b) HUVECs. Data were obtained from analysis of images from time-lapse videos at 20 min intervals. All experiments were performed in triplicate.

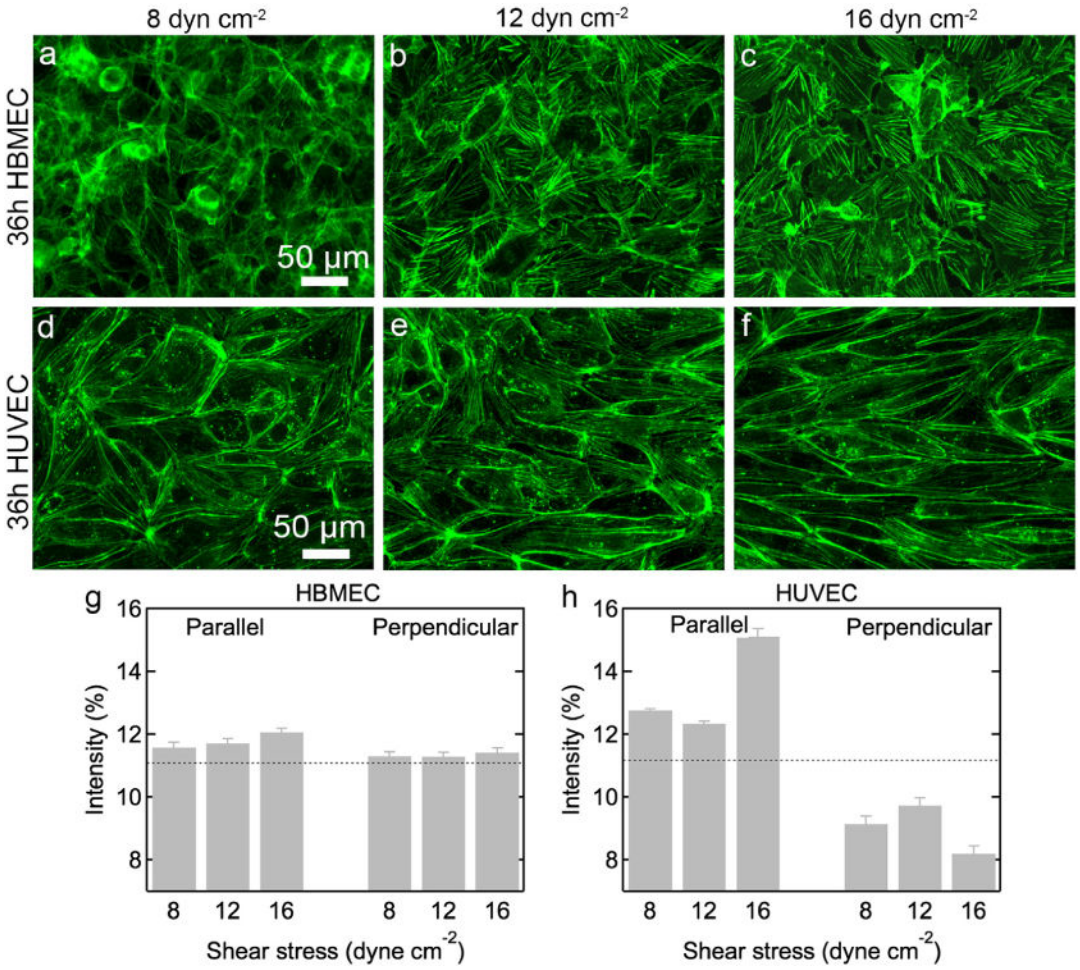

Fig. 6.

Actin filaments in HBMECs are not aligned in the direction of flow under shear stress. Immunofluorescence images and quantitative analysis of actin filament orientation in HBMECs and HUVECs after 36 h. HBMECs: (a) 8, (b) 12, and (c) 16 dyne cm^{-2}. HUVECs: (d) 8, (e) 12, and (f) 16 dyne cm^{-2}. Flow is in the horizontal direction. The intensity of actin filaments parallel (±10°) and perpendicular (±90°) to the flow direction under 8, 12, and 16 dyne cm^{-2} shear stress for (g) HBMECs and (h) HUVECs. The dotted lines represent the intensity (11.1%) for a random distribution of actin filaments. All experiments were performed in triplicate. Error bars represent SE.

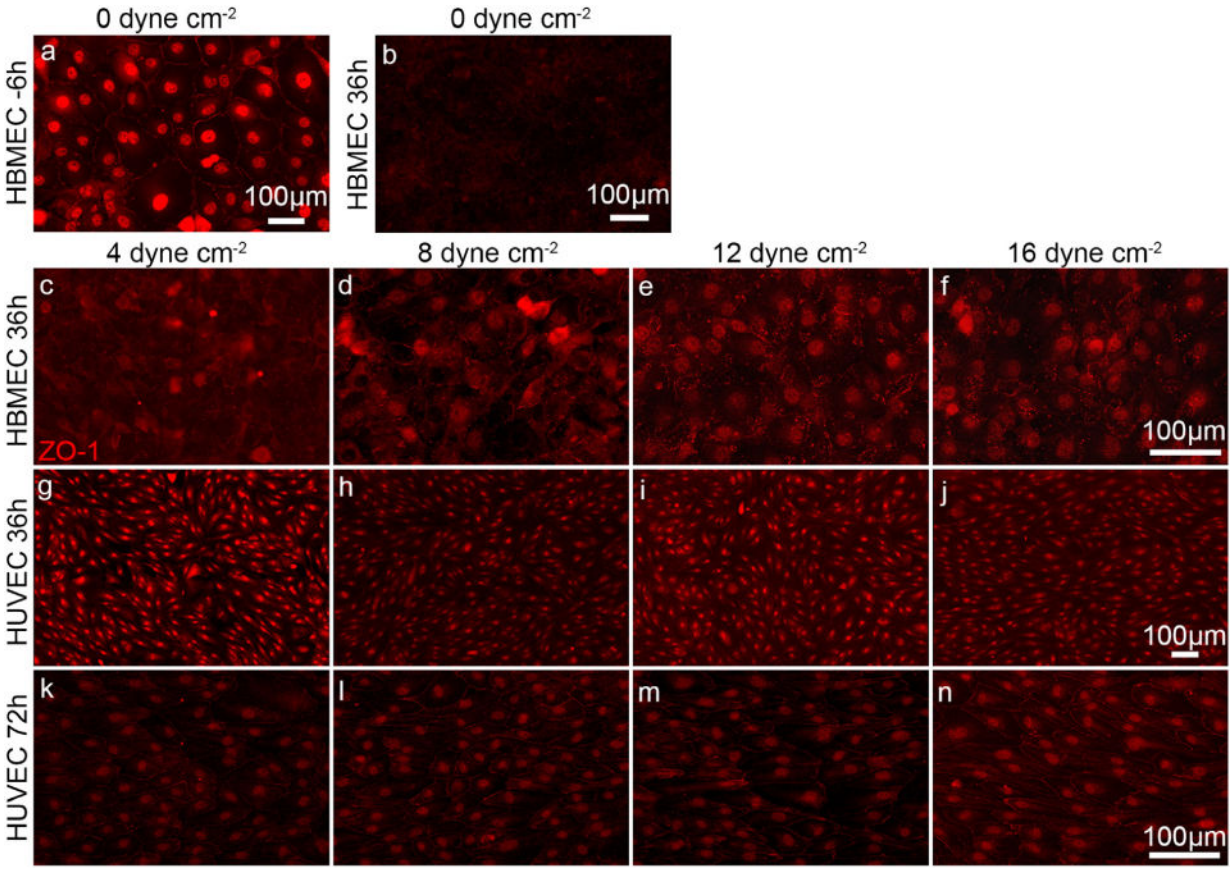

Fig. 7.

Immunofluorescence images showing ZO-1 expression in HBMECs and HUVEC monolayers. HBMECs: (a) on reaching confluence and (b) after 36 h under static conditions. HBMECs after 36 h at (c) 4, (d) 8, (e) 12, and (f) 16 dyne cm^{-2}. HUVECs after 36 h of flow at (g) 4, (h) 8, (i) 12, and (j) 16 dyne cm^{-2}. HUVECs after 72 h of flow at (k) 4, (l) 8, (m) 12, and (n) 16 dyne cm^{-2}.

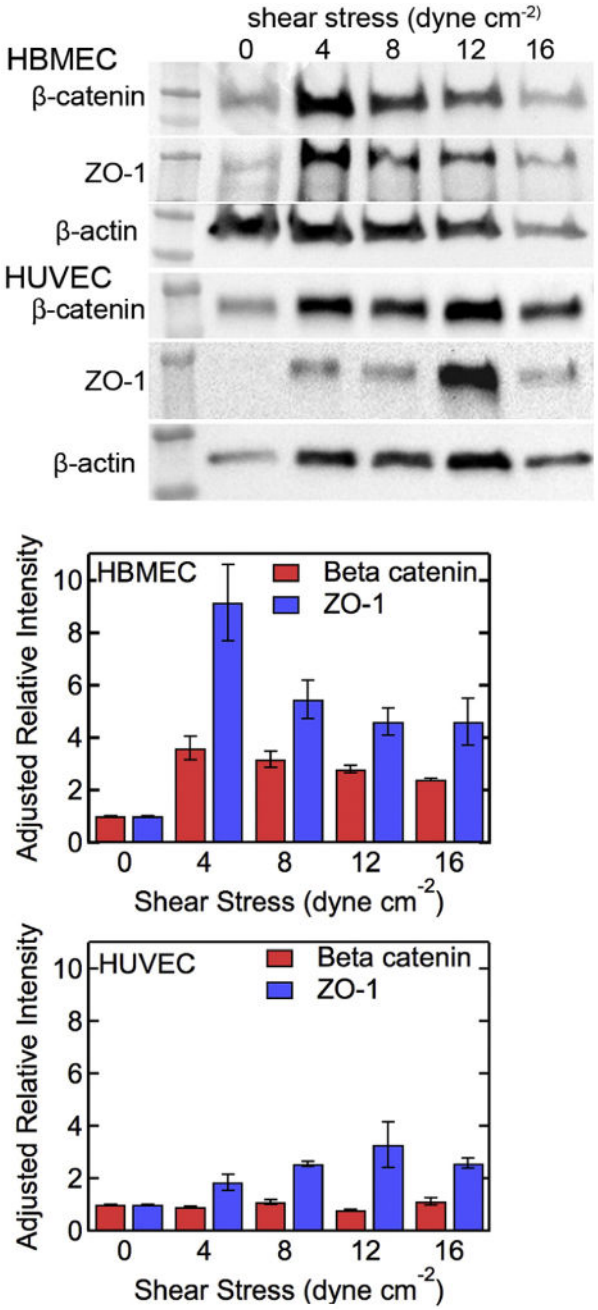

Fig. 8.

Expression of beta-catenin and ZO-1 in HBMEC and HUVEC monolayers. Western blot for (a) beta-catenin, (b) ZO-1, and (c) beta-actin loading control in HBMECs after 36 h under static conditions and under flow. Western blot for (d) beta-catenin, (e) ZO-1, and (f) beta-actin loading control in HUVEC monolayers after 36 h under static conditions and under flow. Adjusted relative expression of ZO-1 and beta-catenin in (g) HBMEC and (h) HUVEC monolayers. All experiments were performed in triplicate. Error bars represent SE.

Table 1

Summary of the morphology of endothelial cells in confluent monolayers subjected to shears stress, and in resected vessels.

Cell line		SS (dyne cm^{-2})	t (h)	C	Err	IAR	Err	θ (deg)	Err	*N*	Comments	Reference
HUVEC	CP	0				0.63					Data from Fig. 2	Blackman (2002)
		7.5	24			0.5						
HUVEC	LF	0		0.56	0.12 (SD)						Data from Table 1	Chiu et al. (1998)
		21	24	0.34	0.14 (SD)							
HUVEC	CP	0		0.73							Data from Fig. 2	Simmers, *Am J Heart Circ Physiol* (2007)
		7.5	96	0.65								
HAAEC	LF/T	18	12	0.38							Data from Fig. 3	Rouleau et al. (2010))
			24	0.36								
BAE	CP	0				0.72	0.02 (SE)	55	3.0 (SE)	60	Data from analysis of microscope images (Fig. 2)	Malek and Izumo (1996)
		20	24			0.24	0.01 (SE)	15	1.6 (SE)	36		
BAE	LF	0		0.77	0.10 (SD)					141	Data from Table 1	Eskin et al. (1984)
		34	21	0.5	0.14 (SD)					140		
BAE	LF	0		0.85		0.66				140–400	Morphological parameters calculated from data in Table 1:	Levesque and Nerem (1985)
		10	24	0.74		0.53				140–400	C from cell area and perimeter; IAR from cell length and width;	
		0		0.9		0.7				140–400	orientation angle from Fig. 4	
		30	24	0.55		0.33				140–400		
		0		0.8		0.62		45		140–400		
		85	24	0.47		0.27		14		140–400		
BAEC	LF	0		0.58				40			Data from Fig. 2	Ensley et al. (2012)
		15	24	0.33				9				
Animal	**Vessel**											
Rabbit	Aorta			0.29	0.01 (SE)	0.14	0.01 (SE)	6.7	0.76 (SE)	52	Data obtained from analysis of microscope image (Fig. 1)	Reidy and Langille (1980)
Rabbit	Aorta			0.25	0.02 (SE)	0.16	0.01 (SE)	4.9	0.9 (SE)	19	Data from analysis of microscope image (Fig. 1)	Silkworth and Stehbens (1975)

Cell line		SS (dyne cm^{-2})	t (h)	C	Err	IAR	Err	θ (deg)	Err	*N*	Comments	Reference
Rabbit	Aorta			0.34		0.17		15			Circularity and average orientation angle from Table 1; IAR calculated from cell length and width (Table 1)	Nerem et al. (1981)
Rat	Aorta					0.2				500	IAR calculated from cell length and width in Table 2	Zand et al. (1988)
Rat	Aorta			0.3	0.02 (SE)	0.19	0.02 (SE)	4.5	0.7 (SE)	20	Data from analysis of Fig. 1	Kibria et al. (1980)
	Aorta					0.18	0.24			310	IAR calculated from cell length and width in Table 2	
	Pulmonary vein					0.48	0.1			184		
Dog	Aorta			0.33	0.02 (SE)	0.19	0.02 (SE)	5.7	0.9 (SE)	20	Data from analysis of microscope image (Fig. 2a)	Levesque et al. (1986)

SS – shear stress, C – circularity ($C = 4\pi A/P^2$), A – cell area, P – cell perimeter, IAR – inverse aspect ratio (cell width/cell length), θ – average orientation angle with respect to the direction of flow, N – number of cells analyzed. BAE – bovine aortic endothelial cells, HUVEC – human umbilical vein endothelial cells, BAEC – baboon artery endothelial cells, HAAEC – human abdominal aortic endothelial cells. CP – cone and plate, LF – linear flow, LF/T laminar flow in a tube.